

Detection of Regional Mechanical Activation of the Left Ventricular Myocardium using High Frame Rate Ultrasound Imaging

Kaja F. Kvåle, Jørn Bersvendsen, Espen W. Remme, Sebastien Salles, John M. Aalen, Pål H. Brekke, Thor Edvardsen and Eigil Samset

Abstract—We have investigated the feasibility of noninvasive mapping of mechanical activation patterns in the left ventricular (LV) myocardium using high frame rate ultrasound imaging for the purpose of detecting conduction abnormalities. Five anesthetized, open chest dogs with implanted combined sonomicrometry and electromyography (EMG) crystals were studied. The animals were paced from specified locations of the heart, while crystal and ultrasound data were acquired. Isochrone maps of the mechanical activation patterns were generated from the ultrasound data using a novel signal processing method called Clutter Filter Wave Imaging (CFWI). The isochrone maps showed the same mechanical activation pattern as the sonomicrometry crystals in 90% of the cases. For electrical activation, the activation sequences from ultrasound were the same in 92% of the cases. The coefficient of determination between the activation delay measured with EMG and ultrasound was $R^2 = 0.79$, indicating a strong correlation. These results indicate that high frame rate ultrasound imaging processed with CFWI has the potential to be a valuable tool for mechanical activation detection.

Index Terms— Animal study, Clutter Filter Wave Imaging, Electrical activation, High Frame Rate Echocardiography, Mechanical activation, Pacing.

I. INTRODUCTION

CARDIAC electrical conduction abnormalities can cause contraction abnormalities and reduce the ability of the heart to perform its purpose; to pump blood through the

Manuscript submitted September 24, 2018. This work was supported by the Norwegian Research Council through the Center for Cardiological Innovation (CCI).

K. F. Kvåle and E. Samset are with the Center for Cardiological Innovation (CCI), Oslo University Hospital, Oslo, Norway, the University of Oslo, Oslo, Norway and GE Vingmed Ultrasound, Horten, Norway. (e-mail: kaja.kvale@ge.com, eigil.samset@ge.com)

J. Bersvendsen is with the Center for Cardiological Innovation, Oslo University Hospital, Oslo, Norway and GE Vingmed Ultrasound, Horten, Norway.

E. W. Remme and J. M. Aalen are with the Institute for Surgical Research, Oslo University Hospital and the Center for Cardiological Innovation, Oslo University Hospital, Oslo, Norway.

S. Salles is with the Norwegian University of Science and Technology, Trondheim, Norway.

P. Brekke is with the Center for Cardiological Innovation, Oslo University Hospital, Oslo, Norway.

T. Edvardsen is with the Center for Cardiological Innovation Oslo University Hospital and the University of Oslo, Oslo, Norway.

circulatory systems of the body[1]. The contraction of a normal heart is the result of a coordinated effort of myocardial fibers that have been electrically activated in a specific sequence[2, 3]. Mechanical activation follows milliseconds after electrical activation and has been shown to propagate in a pattern that correlates well with the electrical activation pattern[3, 4]. Thus, being able to track regional mechanical activation of the left ventricle (LV) through non-invasive imaging, has the potential to give valuable information about arrhythmic conditions, cardiomyopathies, dyssynchrony and pacing. Detailed knowledge of the timing and pattern of mechanical activation could be useful in characterizing dyssynchrony for prediction of response to cardiac resynchronization therapy[5], and for determining the source of a focal arrhythmia[6, 7] or a reentrant arrhythmia.

In clinical practice, noninvasive detection and diagnosis of cardiac electrical activity is performed with a 12-lead electrocardiogram (ECG). However, this technology measures the cardiac electrical activity on the surface of the body and has limited spatial resolution for accurately determining regional electrical activity in the heart[8]. Electrocardiographic imaging (ECGI) was developed to map the electrical activity of the heart at high spatial resolution [9]. This technique gives detailed three-dimensional (3D) maps of the electrical activation of the heart but is time consuming and requires special hardware in the form of a multi-electrode vest and magnetic resonance (MR) and/or computed tomography scans for geometrical information [10]. There have also been developments in mechanical activation detection using MR imaging. MR tagging has been shown to be able to non-invasively map the mechanical activity of the LV [11], but the technique is not able to capture short-lived early systolic events due to the current limitations in frame rate [4]. Nevertheless, non-invasive, radiation free imaging methods remain to be put into clinical use. Invasive procedures currently employed in the clinic are typically catheter-based, such as electrophysiology contact mapping. This procedure results in ionizing exposure and prolonged sedation or anesthesia for the patient, in addition to being time consuming and costly[12]. A safe, time effective and non-invasive method for regional electrical activation mapping would therefore be advantageous.

Echocardiography is already an established part of the routine examination of the patient's heart. In recent years, developments in ultrasound technology have allowed for a

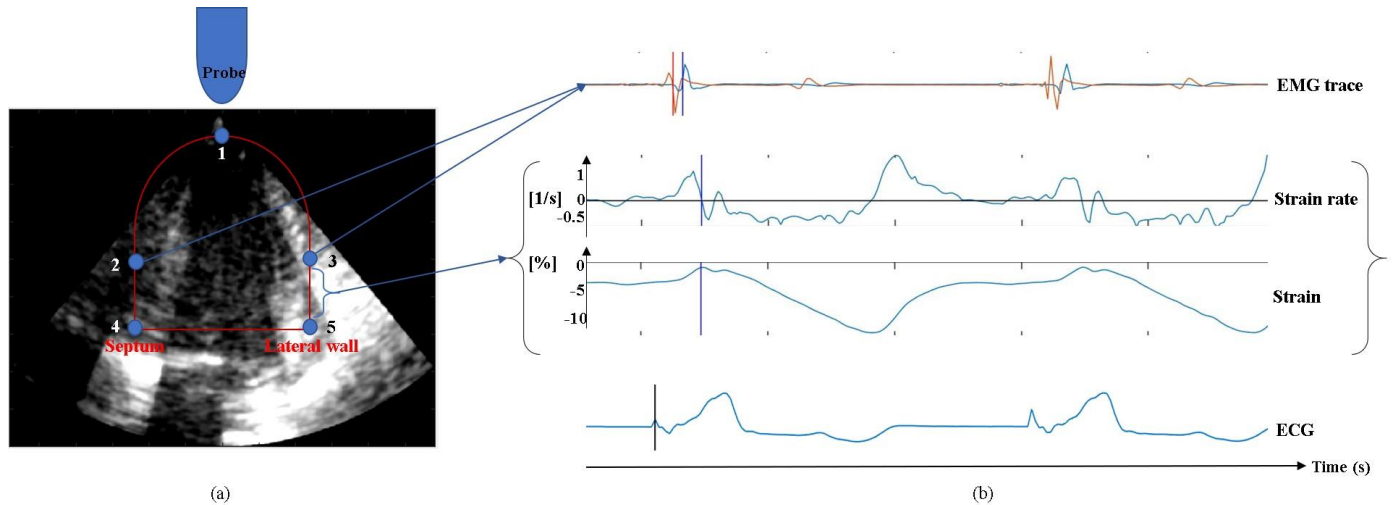


Fig. 1: Crystal placement and analysis. (a) The targeted placement of the crystals in the LV and the imaging plane for the apical 4 chamber view. (b) The electrical and mechanical activation detection from crystals. The top plot shows EMG traces from crystal 2 in blue and crystal 3 in red, the red and blue vertical lines mark the time of electrical activation. The two middle plots show the strain rate and strain recorded from crystal pair 3 and 5. Mechanical activation is marked with a blue vertical line where the strain rate curve crosses zero on the y-axis. The bottom plot shows the ECG trace. The vertical line shows the time of pacing.

substantial increase in frame rate. Up to several thousand frames per second can now be acquired, compared to the conventional rate of 50-200 frames per second. This allows for the study of short lived events that are often lost between frames with conventional ultrasound imaging[13], such as the activation of the heart[14]. Electrical activation cannot be directly determined by imaging, but it has been shown that mapping the mechanical activation pattern by analyzing tissue motion is possible with high frame rate ultrasound images[12, 15, 16].

Previously published studies on mechanical activation detection with ultrasound have used strain rate to derive the timing of mechanical activation, such as the technique called Electromechanical Wave Imaging [16]. Strain rate is the spatial derivative of tissue velocity and is susceptible to noise[17], and thus, requires substantial smoothing and filtering. Various motion estimators have been applied to perform tissue velocity estimation. The most used are phase-based methods[18], such as Tissue Doppler Imaging (TDI), and cross correlation (CC) methods[19].

In this work we have used a novel signal processing method called Clutter Filter Wave Imaging (CFWI). CFWI has multiple advantages over other techniques that aim at mapping tissue velocities. Indeed, in part because it does not attempt to quantify tissue motion itself, CFWI benefits from improved SNR and low computational cost when compared against TDI [20] and CC, respectively. CFWI consists of applying a clutter filter, i.e. high pass filter, on the beamformed data and using the transition band of the filter to attenuate the velocities of interest thereby determining activation from the motion of the attenuated band. CFWI has been compared to other motion estimators and has been shown to perform better in the apical regions of the heart, and to have a better signal-to-noise ratio when applying the same averaging and smoothing filter[20].

Several studies have been published on using strain rate and high frame rate imaging to detect and visualize the mechanical activation of the myocardium in sinus rhythm[21], including studies with induced pacing to simulate arrhythmias in the

heart[12, 15]. However, most studies have compared their findings only to electrical activation. In this study, we assessed the feasibility of using high frame rate imaging processed with CFWI to detect regional mechanical activation in an animal model. Data was acquired during pacing from different sites around the ventricles, and the results from ultrasound were compared to both electrical and mechanical activation measured by combined electromyography (EMG) and sonomicrometry crystals, respectively.

II. METHODS

A. Animal Preparations

Five male, mongrel dogs of body weight 42 ± 5.5 kg were anesthetized by propofol and opioids (single dose methadone 0.2 mg/kg, followed by propofol 3-4 mg/kg and a bolus of fentanyl 2-3 μ g/kg, thereafter continuous infusion of propofol 0.2-1 mg/kg/min and fentanyl 5-40 μ g/kg/hour). The animals were artificially ventilated through a cuffed endotracheal tube and surgically prepared with a median sternotomy followed by partial splitting of the pericardium from apex to base. The edges of the pericardial incision were loosely resutured after instrumentation. The ECG was monitored from limb leads. The National Animal Experimentation Board approved the study and the animals were supplied by the Center for Comparative Medicine (Oslo University Hospital, Rikshospitalet, Oslo, Norway).

B. Data Acquisition

In line with the principle of “replacement, reduction and refinement”, the animals were part of multiple studies. For this reason, the pacing protocols varied somewhat between the animals. Table I summarizes the acquired data in each animal.

1) Dimensions and Electromyograms

LV dimensions were measured as longitudinal segment lengths by sonomicrometry using 2 mm diameter crystals (Sonometrics Corporation, London, Ontario, Canada) implanted in the inner third of the myocardium in the

TABLE I
OVERVIEW OF DATA COLLECTION

Animal #	Pacing	Acquisitions not used
1	BS, RV, LV, BiV	The sonomicrometry crystals were disturbed by the presence of the ultrasound probe for BS and LV pace.
2	BS, RV, LV, BiV	The sonomicrometry crystals were disturbed by the presence of the ultrasound probe for RV, LV and BiV pace. It was not possible to acquire normal apical 4-chamber views in this animal due to difficulty in placing the probe. The resulting CFWI velocity images from RV, LV and BiV pacing were not of high enough quality for further analysis. Manual selection of the mechanical activation was possible on the ultrasound data from BiV pacing.
3	BS, RV, LV, Septum	
4	BS, RV, LV	
5	BS, RV, LV, BiV	Ultrasound data were only stored of BS and RV pace because of a memory limitation on the scanner that was discovered in post processing. The sonomicrometry crystals were disturbed by the ultrasound probe for all acquisitions as the effect of the probe was unknown at the time.

BS = Baseline sinus rhythm, RV = Right ventricle pace, LV = Left ventricle pace, BiV = Bi-Ventricular pace.

interventricular septum and lateral LV walls. The septal crystal was inserted through a small needle channel. Ultrasound guidance was used to ensure optimal positioning. Fig. 1a shows the targeted placement of the ultrasonic crystals in an apical 4-chamber view. The ultrasonic crystals were combined with a bipolar electrode for recording of intramyocardial electromyograms (EMG). This enabled simultaneous assessment of myocardial electrical and mechanical activation. The pacing electrodes were placed in the mid-free wall in the right ventricle (RV), the mid-free wall in the LV and in the mid-septum. Data were sampled at 200 Hz.

2) Echocardiography

Ultrasound data were acquired during sinus rhythm, RV, LV, septal and biventricular (BiV) pacing. Apical 4-chamber views focused on the LV were acquired with a 2.8 MHz center frequency phased array probe connected to a modified GE Vivid E95 ultrasound system. Steered plane wave imaging was used to record beamformed IQ-demodulated (IQ) data at 1000 to 1200 frames per second. 4 to 6 transmit beams per image were used without compounding. Surface ECG was acquired simultaneously with ultrasound imaging and was monitored from limb lead at a rate of 600Hz.

C. Experimental Protocol

Crystal data was recorded immediately prior to echocardiography. A subdiaphragmal access was used to optimize the acquisition of apical images. Plenty of gel was applied between the probe and heart in order to ensure acoustic coupling while limiting mechanical contact between the probe and the heart in order to minimize potential mechanical disturbances of the heart motion by the probe. A protocol of sinus rhythm (n = 5), RV free wall pacing (n = 4),

LV free wall pacing (n = 3), BiV (n = 2) and septal (n = 1) pacing was followed.

The echocardiography acquisition sequence lasted for about two seconds. The animals had a heart rate ranging from 100 to 120 bpm, which resulted in at least 2 heart cycles per data acquisition. There was no ECG gating. The images were stored from the time an acquisition button was pressed. The implanted crystals were not visible in the ultrasound image. Pacing was sustained until both the sonomicrometry/EMG acquisition and the echocardiographic acquisition were finished. The recordings were performed during the same breath-hold with a respirator to ensure that the heart rhythm and ECG morphology were the same for both data sets. All recordings were performed during stable conditions with the ventilator off to avoid respiratory motion artifacts. The ventilator was off for a maximum of 30 seconds while both recordings were performed.

Data analysis was performed off-line using MATLAB (The MathWorks, Natick, MA, USA). Processing time for isochrone map generation was approximately 5 minutes per data set.

D. Data Analysis

1) Activation measured from crystals

The EMG crystals measured the timing and voltage of the depolarization wave as it arrived at the location of the crystals. EMG was measured at crystals 2 and 3 in the mid-septum and mid-lateral wall, respectively (Fig. 1a). Electrical activation was defined as the time point between the largest deflections in the EMG trace[5, 22] (Fig. 1b).

Myocardial strain was obtained from segment length measurements of sonomicrometry crystal pairs, and strain rate was calculated as the time derivative of strain. Four crystal pairs, two for each LV wall, were used for the assessment of mechanical activation. The placements were mid to base (crystal pair 2-4 and 3-5, Fig. 1a) and mid to apex (crystal pair 1-2 and 1-3, Fig. 1a). Mechanical activation for a crystal pair segment was defined as the change in curvature for the strain curve and the point of zero crossing - which often coincided with the maximum acceleration - of the strain rate curve[5] (Fig. 1b).

The time of pacing was assessed from the ECG trace (Fig. 1D) as the time of the Q-wave. The time of pacing, electrical and mechanical activation were manually selected in a plot, and all measurements were averaged over at least three heart cycles. Pacing time was decided first and used as a reference time for the other events.

2) Clutter Filter Wave Imaging

The principle of CFWI is shown in Fig. 2. In blood flow, a clutter filter is generally used to reject all tissue motion from the data. The principle of CFWI, however, is to track certain tissue velocities by attenuating them using a high pass clutter filter. The filter will attenuate all velocities below the cutoff equally (Fig. 2). The resulting B-mode image series, after filtering, will display mechanical waves propagating as dark bands [20]. No tracking was performed on the B-mode image.

The outputs from the CFWI method were defined here as CFWI velocity and CFWI acceleration (Fig. 3b). To achieve CFWI velocity, a temporal clutter filter was first applied to the IQ-data. A third order high-pass Butterworth filter with a

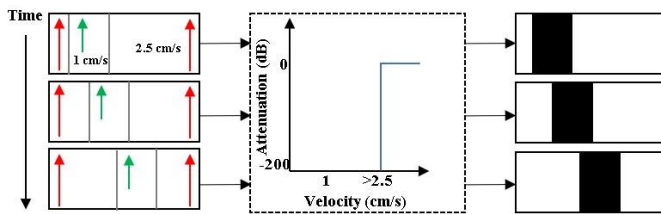


Fig. 2: Clutter Filter Wave Imaging principle. A medium with two axial velocities (1 cm/s in green and >2.5 cm/s in red) is filtered with a high pass filter with cutoff velocity >2.5 cm/s. The resulting medium will contain a black region, which corresponds to the removed 1 cm/s.

cutoff frequency of 114 Hz corresponding to a cutoff velocity of 2.5 cm/s was used. The cutoff velocity was roughly the maximum tissue velocity for the relevant time interval[20]. The normalized cutoff velocity is defined as

$$f_{Cutoff} = \frac{v_{Cutoff}}{vNyq} \quad (1)$$

with

$$vNyq = \frac{c_0 * FPS}{4f_0} \quad (2)$$

where v_{Cutoff} is the cutoff velocity, c_0 is the speed of sound, FPS is the frame rate, f_0 the transmit frequency, and $vNyq$ the Nyquist velocity.

The absolute value of the filtered IQ-data was envelope detected. Then, the Signal to Noise Ratio (SNR) was improved by performing spatiotemporal averaging. Here we used a mean sliding window smoothing over 5 mm in the axial direction, 7 beams in the lateral direction and 11 frames in time. The result was a B-mode image sequence with attenuated tissue velocities. The trace for one myocardial spatial point was similar to the absolute value of a myocardial velocity trace, although the CFWI velocity should not be confused with actual velocity. The CFWI velocity is still filtered B-mode intensities.

The CFWI acceleration was achieved by differentiating the CFWI velocity with respect to time. CFWI velocity and acceleration were then used to determine the mechanical activation pattern of the LV.

3) Mechanical Activation Detection with CFWI

In an LV myocardial velocity trace (Fig. 4, top plot), there is a negative wave caused by atrial induced filling, followed by a positive pre-ejection spike as the LV myocardium contracts to close the mitral valve[23]. In between, the LV has been mechanically activated and wall shortening has started. The pre-ejection spike in the velocity trace corresponds to a positive peak in the CFWI velocity trace. This was used to define the mechanical activation as the maximum acceleration of the pre-ejection spike in the TDI trace and the peak CFWI acceleration. An algorithm was developed to automatically define mechanical activation for every spatial point of the LV. The steps of the algorithm are outlined in Fig. 3c and examples of the analysis in steps 3 and 4, of Fig 3c, are shown in Fig 4 and in supplementary videos in the appendix available at <http://ieeexplore.ieee.org>.

First, the LV was manually segmented to achieve a shorter computation time. Hence, mechanical activation was only detected for the spatial points in the segmented area. Second, the onset of the Q wave was manually defined in the ECG trace and used as the start of the search window. The end of the search window was set to 130 ms after the start. This duration was selected to be sure to have the whole QRS complex within the search window. Third, a threshold for the minimum intensity of the CFWI velocity was set to define the first possible time of mechanical activation (shown in Fig. 4, CFWI velocity plot). This value ranged between 0.25 and 0.6 dB, due to the differences in intensity of the different data sets. The threshold was set manually for each data set. Finally, the first occurrence of the threshold value of the CFWI velocity was detected within the search window, and the time of peak CFWI acceleration was found only after the CFWI velocity had reached the threshold (the time of activation is shown for TDI velocity, CFWI velocity and acceleration and ECG in Fig. 4). If the threshold was never reached within the search window no mechanical activation was found for that spatial point. An isochrone map with the time of mechanical activation for every spatial point of the LV was the result.

In the case where the algorithm gave an isochrone with large discontinuities, the CFWI and time derivative traces were plotted and, if possible, the mechanical activation times were manually selected. One cardiac cycle was considered for each data set.

III. RESULTS

A. Sensitivity analysis for CFWI filter cutoff velocity and threshold

The sensitivity of the selected filter cutoff velocity and the threshold used for mechanical activation detection from CFWI velocity was investigated for 6 of the acquisitions and shown in Fig. 5. Isochrones were generated for different cutoff velocities or thresholds while all other parameters were kept the same, such as the search area and the area of the walls the activation times were selected from. In the figure, the activation time for the cutoff velocity or threshold used was defined as 0%, while the activation time for other cutoff velocities were calculated as the percent deviation from the original activation time.

The top plot shows the activation time between walls (y-axis) plotted against the filter cutoff velocity (x-axis). The activation times are fairly stable from 2.5 cm/s and up to 4 cm/s. Above 4 cm/s and below 2.5 cm/s the variation in activation times is not negligible.

The bottom plot shows the activation time plotted against the CFWI threshold used for mechanical activation detection. The range of thresholds used in the analysis (0.25 dB to 0.6 dB) is marked in the plot with red circles.

B. Isochrones

Mechanical activation was visualized using isochrone maps where 0 ms corresponded to the onset of the QRS complex and a blue to red color spectrum was used to display early to late activation. The lower value of the colorbar was set to zero as it was the start of the search window, and the higher value was automatically set to the highest mechanical activation

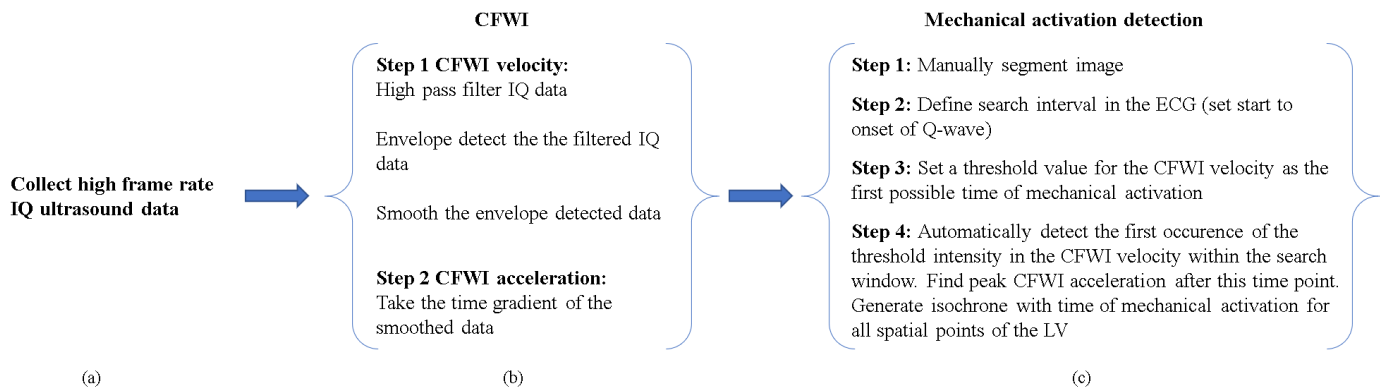


Fig. 3: Flow chart for the ultrasound analysis. (a) High frame rate ultrasound IQ data acquisition. (b) CFWI analysis. (c) Mechanical activation detection.

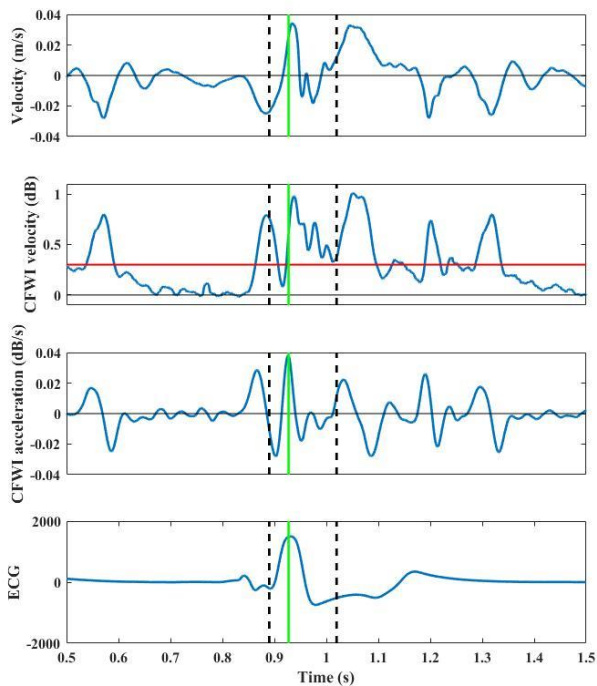


Fig. 4: Mechanical activation analysis for one spatial point in the septum during RV pacing. The top plot shows the velocity estimated using TDI. The next plot shows the CFWI velocity curve, below is the CFWI acceleration curve and at the bottom the ECG. The search area is marked with vertical black dashed lines, the CFWI threshold is shown in the CFWI velocity plot with a red horizontal line and the green vertical lines show the time of activation.

value found in the isochrone. Adjustment of the higher value was done to remove clear outliers. The colorbar was then adjusted to the largest value within each pacing case for an easier comparison. Manual selection of activation times for large discontinuities was performed for smaller areas in 3 out of 13 isochrones.

1) Baseline Sinus Rhythm

During sinus rhythm there was a relatively short activation period as seen by the narrow color spectrum in each of the five animals (Fig. 6) though there was some variation in the mechanical activation pattern between the animals. The acquired view for animal #2 was more medial, close to a long axis view, due to difficulty in placing the probe correctly for this animal.

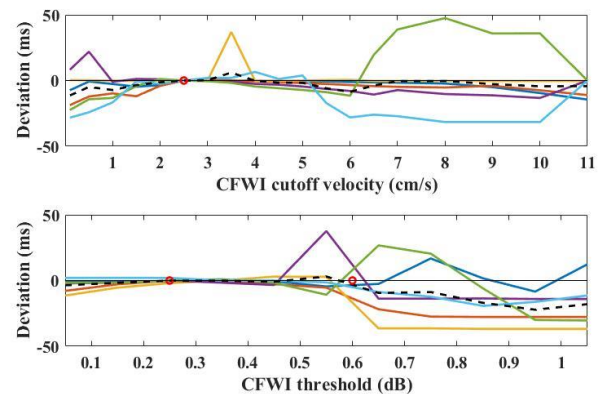


Fig. 5: Sensitivity analysis for 6 of the 15 data sets. All y-values are deviations from the activation time found for the cutoff velocity or CFWI threshold used for a data set. For CFWI filter cutoff velocity 2.5 cm/s the deviation is always zero. Top: shows the deviation from the activation time plotted against the CFWI filter cutoff velocity. Bottom: shows the deviation from the activation time plotted against the CFWI threshold. The black dashed lines are the averages of the 6.

2) RV pacing

During RV pacing mechanical activation started in the mid to apical septum and then spread towards the lateral wall of the LV and towards the basal septum as seen in Fig. 7a. The figure shows the isochrones obtained from three of the four animals with this pacing protocol, while in the fifth animal the images were too noisy for an isochrone map to be created.

3) LV pacing

During LV pacing, the LV free wall was mechanically activated before the septum as shown in Fig. 7b, displaying the 3 animals with this pacing intervention. In one of the animals, the mechanical activation appeared first in the mid lateral wall of the LV, while for the two others, early activation was observed in the basal lateral wall. Some noise appears in the basal regions of the lateral wall.

4) Septal and BiV pacing

Fig. 7c and d show the isochrones obtained from septal and BiV pacing, respectively. The isochrone from septal pacing (Fig. 5c) showed early activation in the basal septum, but also some early activation in the apical septum, with late activation in the basal lateral wall. For BiV pacing (Fig. 7d) early activation was observed in the mid-lateral wall and in the mid

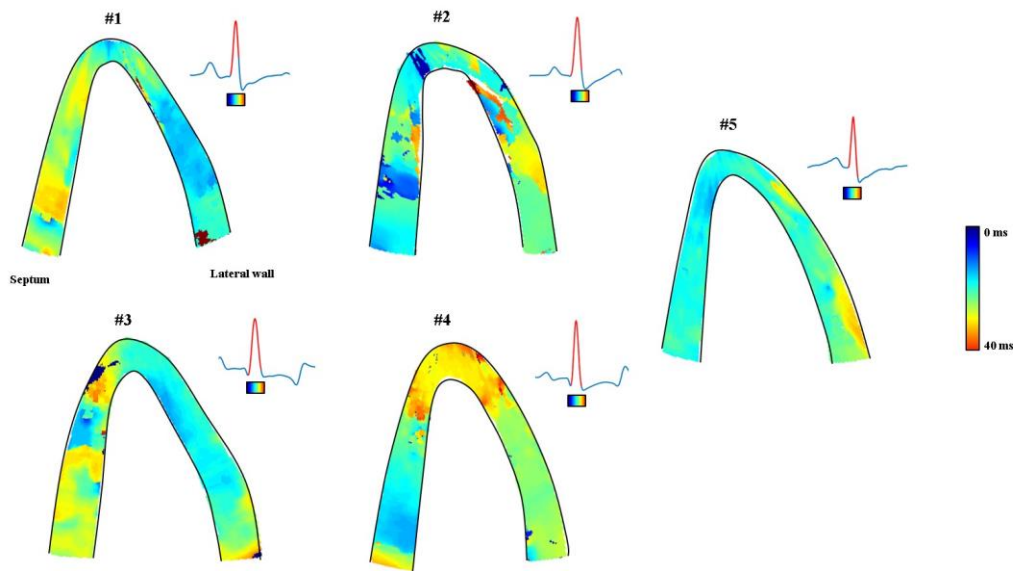


Fig. 6: The isochrone maps obtained from all animals in sinus rhythm. 0 ms is at the onset of the QRS complex. The red part of the ECG marks the duration of the activation and shows the start and end point of the colorbar. For animals 1 and 3 early activation was observed in the lateral wall, and later activation in the septum. For animals 4 and 5, the earliest activation was observed in the septum, towards the base for animal number 4 and apically for animal number 5. Animal number 4 showed the latest activation in the apex, while in animal number 5 the activation was later in the epicardial lateral wall. For animal number 2, the early activation started in the septum and later activation in the lateral wall. The view for animal 2 was closer to a parasternal/apical long axis view due to difficulties in placing the probe correctly, which is also reflected in the segmentation of the LV.

to apical septum. Later activation spread from the early activation sites towards the basal lateral wall, the apex and the basal septum. BiV pacing was also performed in a second animal, but due to poor image quality it was not possible to create an isochrone from this image series.

C. Comparison of reference method and CFWI

Table II shows the comparison of mechanical activation patterns derived from sonomicrometry and CFWI, the sequence of electrical activation from EMG, and the activation delay between walls measured with EMG and with CFWI. The sequence of septum to lateral wall activation was used as a positive activation delay. The isochrones were used for the measurements from the ultrasound results. For the activation delay, areas corresponding to the EMG crystals were considered, while for the activation sequence, areas corresponding to the sonomicrometry segments were considered (Fig. 1a). The pixels from the selected areas in the isochrones were averaged to find one activation time for the area.

In total, 10 cases were available for mechanical activation sequence comparison, and 13 cases were available for electrical and mechanical activation delay comparison. For the remaining cases the sonomicrometry crystals had been disturbed by the presence of the ultrasound probe (5 cases), or the ultrasound images were too noisy which gave CFWI velocity images that were too difficult to interpret (1 case, and a second case where a full isochrone map could not be generated but manual measurements were performed). The mechanical activation pattern determined with CFWI was found to be the same as the mechanical activation patterns from the sonomicrometry crystals in 9 out of 10 (90%) cases. Furthermore, when considering only the electrical activation patterns 12 out of 13 (92%) cases showed the correct activation sequence compared to the EMG crystals.

Linear regression analysis of the activation delay measurements between the reference method, EMG, and CFWI gave a strong correlation ($R^2 = 0.79$) (Fig. 8a). Furthermore, the mean of the methods and the difference of the methods were plotted in Fig. 8b. A slope was observed in the Bland-Altman plot. For small activation delays the measured electrical and mechanical activations were similar. While for an increasing activation delay (both positive and negative), the mechanical activation delay increased even more than the electrical activation delay.

D. Repeatability

Fig. 9a shows isochrones, from animal #1, from two consecutive heart cycles during baseline, RV and LV pacing. Fig. 9b shows histograms of the absolute differences in activation time between consecutive heart cycles for all acquisitions during baseline, RV and LV pacing. For the baseline isochrones, 93.7 % of the difference in activation time from two heart cycles was below 5 ms (Fig 9b, left). For RV pacing, 97.3 % of the difference in activation time from two heart cycles was below 5 ms (Fig. 9b, middle), while for LV pacing, 93.3 % of the differences were below 5 ms (Fig 9b, right).

IV. DISCUSSION

In this study we developed and tested a novel method for non-invasive echocardiographic assessment of regional mechanical activation of the LV myocardium. We analyzed the mechanical activation patterns from five open chest animals during baseline sinus rhythm, RV, LV, BiV and septal pacing. From the isochrone maps generated using the CFWI method, we were able to detect the approximate origins of the paced beats and recover the correct activation sequences compared to sonomicrometry in 9 out of 10 cases. When

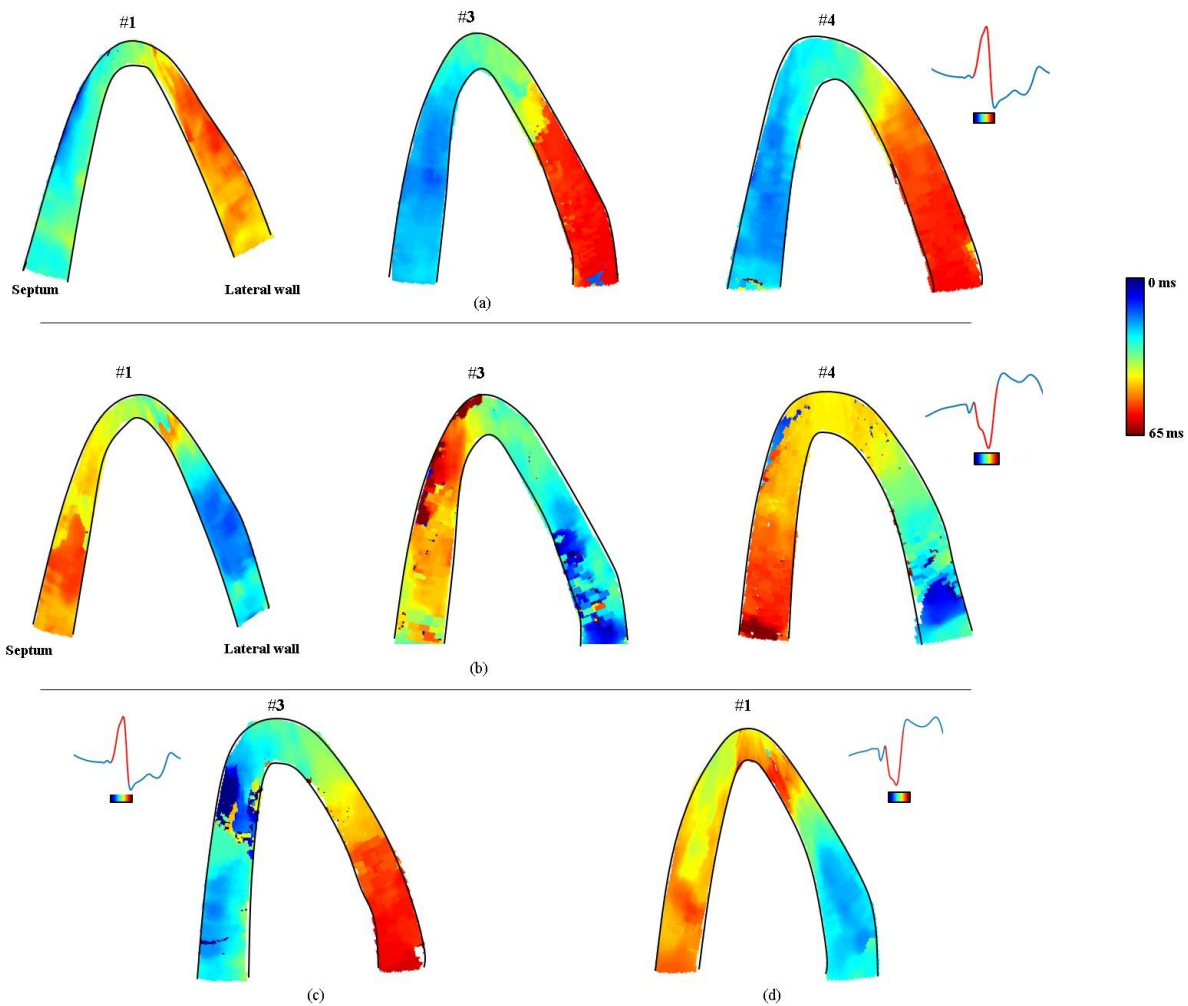


Fig. 7: The start of the isochrone maps is the onset of the QRS complex in the ECG. The red part of the ECG marks the duration of the activation and shows the start and end point of the colorbar. (a) RV free wall pacing from three animals. The pacemaker was placed approximately in the mid-RV free wall. All three animals displayed the same pattern of activation, with early activation in the mid-septum and late activation in the lateral wall. (b) LV pacing from three animals. The pacemaker was placed approximately epicardially on the mid-LV free wall. All three animals displayed an earlier activation in the lateral wall than in the septum. (c) Septal pacing from one animal. The approximate location of the pacemaker was in the mid-septum. Early activation was seen in the basal septum. In the apical septum there was an area of noisy estimates, and an area of early activation. The propagation of activation then continued towards the basal lateral wall. (d) BiV pacing from one animal. The approximate locations of the pacemakers were in the mid-RV free wall and epicardially on the mid-LV free wall. The earliest activation was observed in the mid-lateral wall, but there was also a relatively early activation area in the mid to apical septum. Late activation was found in the apex and in the basal septum.

comparing with electrical activation, the correct activation sequence was found in the isochrone maps in 12 out of 13 cases. We demonstrated very good repeatability for all acquisitions for consecutive cardiac cycles. There was a good agreement between the activation delay measured with EMG and with ultrasound.

Another well-known and much reported method for mechanical activation detection, Electromechanical Wave Imaging [3, 16], estimates the mechanical activation from strain rate calculated from ultrasound data. We chose to validate our CFWI-based method against sonomicrometry crystals, as both the acquisition and the analysis of electrical and mechanical activation was completely independent from the ultrasound acquisition and analysis. Moreover, sonomicrometry crystals have been reported used several times for the assessment of mechanics in animal studies [5, 24] and is an established reference standard.

Table I summarized the collected data. Baseline, RV and LV pacing were performed for all animals, while septum or

BiV pacing was only performed for some animals. The animals from which data were acquired were part of another, yet unpublished, study, in which the pacing protocols varied somewhat between animals. Some sonomicrometry crystal acquisitions were discarded because of disturbance from the ultrasound probe. This effect was noticed during post processing, and therefore some acquisitions had probe disturbances and others did not.

In this paper, we chose to set the cutoff velocity for the CFWI clutter filter to 2.5 cm/s. This value was found by estimating the tissue velocity using TDI and finding the approximate maximum value in the relevant time interval. The maximum value of the tissue velocity was chosen so that all tissue velocities would be attenuated as much as possible. The same cutoff velocity has been used in a previous study researching natural mechanical waves occurring before the QRS-complex[20]. The target for this study was to be able to find the pre-ejection spike in the CFWI velocity trace. A higher cutoff velocity gave a more attenuated CFWI velocity

TABLE II
ELECTRICAL AND MECHANICAL ACTIVATION SEQUENCES AND ACTIVATION DELAYS FROM CRYSTAL DATA AND CFWI

Pacing	Animal #	EMG sequence	Sonomicrometry sequence	CFWI sequence	Δ EMG (ms)	Δ CFWI (ms)
BS	1	SM, LM	-	LB, LA, SA, SB	12.8±1.3	-14.9
	2	SM, LM	SB, SA, LA, LB	Same	13.2±0.8	14.9
	3	LM, SM	LA, LB, SB, SA	Same	-6.2±0.9	-12.4
	4	SM, LM	SB, SA, LA, LB	Same	5.4±0.5	12.5
	5	SM, LM	-	SA, SB, LA, LB	5.3±0.8	11.4
RV	1	{SM, LM}	SB, SA, LA, LB	SA activated before SB	20.7±1.7	27.2
	3		SB, SA, LA, LB	Same	25.1±2.2	54.7
	4		SB, SA, LA, LB	Same	16.6±0.2	27.9
	5		-	SB, SA, LA, LB	19.8±1.1	24.9
LV	1	{LM, SM}	-	LB, LA, SA, SB	-29.3±1.6	-35.4
	3		LB, LA, SA, SB	Same	-42.4±0.5	-24.5
	4		LB, LA, SA, SB	Same	-17.2±0.6	-30.9
Septum	3	SM, LM	SB, SA, LA, LB	Same	30.3±0.3	47.4
BiV	1	{LM, SM}	LB, LA, SA, SB	Same	-28.5±2.3	-39.4
	2		-	-	-40.3±0.7	-

SM = mid-septum, LM = mid-lateral wall. SB = basal septum, LB = basal lateral wall, SA = apical septum, LA = apical lateral wall. Δ EMG and Δ CFWI indicates the time from electrical and mechanical activation, respectively, from mid-septum to the mid-lateral wall. A negative value indicates that the LV lateral wall was activated first.

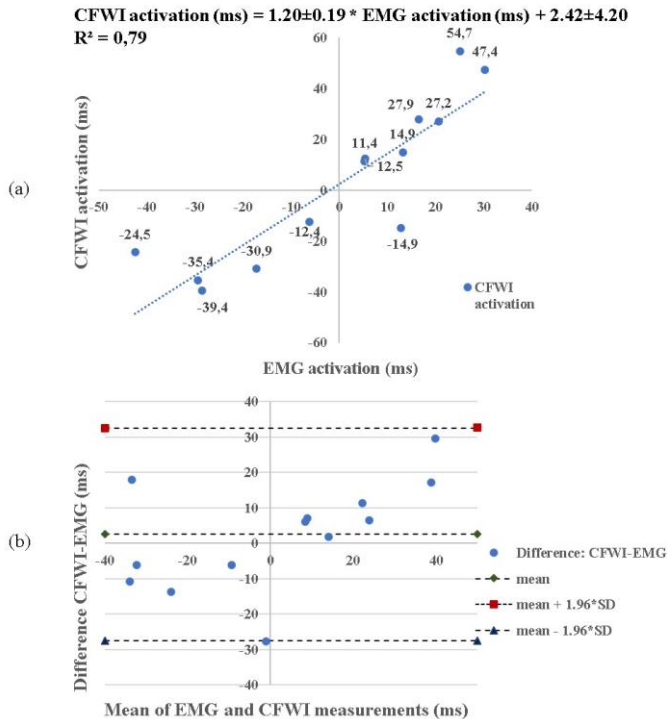


Fig. 8: Comparison of the activation delay measured by EMG and CFWI for each case. The activation sequence of septum to lateral wall was defined as a positive activation delay. (a) Correlation plot showing the correlation between the activation delay measured with EMG and ultrasound. (b) Bland-Altman plot showing the agreement between EMG and ultrasound. An increasing slope indicated that an increasing delay (positive or negative) gave an increasing difference between the mechanical activation delay measured with CFWI and the electrical activation delay measured with EMG.

trace, and a lower cutoff velocity gave a less attenuated trace, both situations made it more difficult to discern the pre-ejection spike. Fig. 5 showed how changing the filter cutoff affected the mechanical activation time between walls for 6 of the acquisitions. The plot showed that the activation measurements were stable for most acquisitions when the cutoff velocity increased above 2.5cm/s, but unstable below. This result showed that the value selected for the cutoff

velocity gave a stable result, and the cutoff was assumed trustworthy in the following analysis.

In this study only apical 4-chamber views focused on the LV were acquired. RV pacing was performed to create maximum dyssynchrony between the walls in the LV. For the resulting isochrones (Fig. 6 and 7), we observed an early activation in the septum for RV and septal pacing, and early activation in the lateral wall for LV and BiV pacing, for all animals, which is consistent with previous studies[3, 12, 15, 25]. The overall qualitative pattern between the three animals for RV pacing were similar, as was the pattern for LV pacing. However, smaller individual differences were observed, as expected, as the pacing sites in each animal were not identical. There are also individual variations in the Purkinje networks, the geometry of the hearts and the imaging planes. The activation pattern observed for RV pacing was fairly similar to the activation pattern found for septal pacing, both in the crystals (EMG and sonomicrometry) and in the isochrones. This was expected as RV pacing and septal pacing generate a qualitatively similar activation pattern in the LV where the septum activates first, before the lateral wall. The resulting LV and BiV pacing activation patterns were also similar. For both LV and BiV pacing, early activation was observed in the lateral wall and late activation in the septum. However, for BiV pacing, the LV and the septum should activate at approximately the same time. This meant that the BiV pacing had not been successful for any of the two animals where sonomicrometry data was available and was in practice an LV pacing. We decided to keep the acquisition in the article because it showed that even though the pacing was unsuccessful, both methods gave the same result. The isochrones from baseline showed short activation times and nearly synchronous hearts as expected. For animal #3 the lateral wall was found to activate before the septum for both the crystals and the isochrone. For animal #1 this pattern was found in the isochrone only. The septum was expected to activate first, but here the differences between the walls were so small that the hearts were synchronous and within the normal range[26]. For animal #2, the view obtained was not a

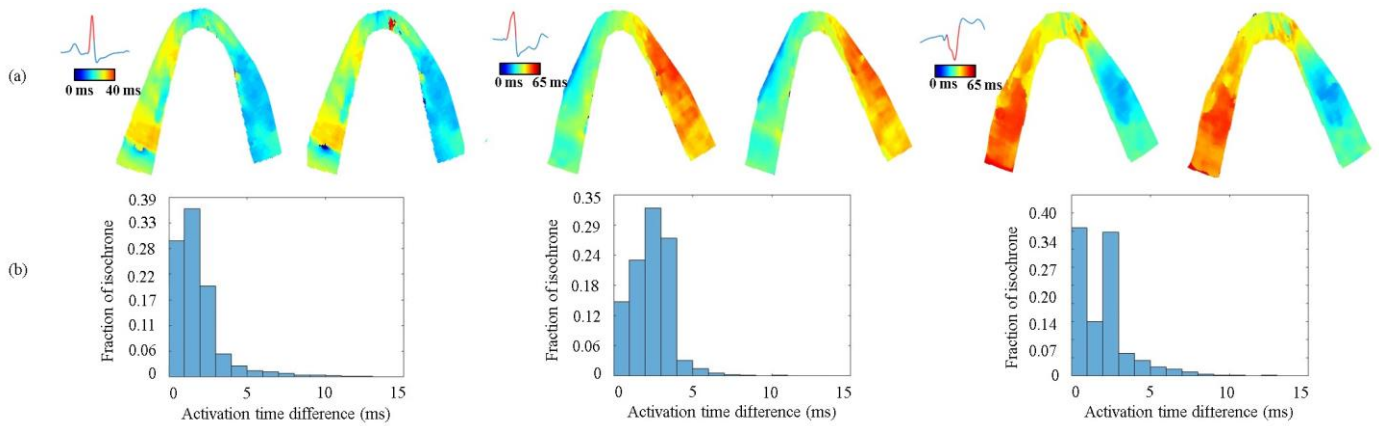


Fig. 9: The repeatability of mechanical activation detection with CFWI. (a): Isochrone maps obtained from two consecutive heart cycles for baseline (left), RV (middle) and LV (right) pacing. (c): The absolute difference between consecutive heart beats were plotted in histograms for all baseline acquisitions (left), RV acquisitions (middle) and LV acquisitions (right).

normal 4-chamber view and thus the segmentation of the LV is an approximation.

In addition to the isochrones, we found good correlation for the activation delay measured with ultrasound compared to the EMG. Fig. 8b showed an increasing slope indicating that the difference between the mechanical activation delay and the electrical activation delay increased with increasing activation delay. This is consistent with previous studies showing that late activated segments have a longer duration from electrical activation to onset of shortening compared to early activated segments[24]: During early systole the pressure gradually increases faster and faster (dP/dt). A segment must generate active force faster than the rise of the applied load in order to shorten. The later a segment is activated, the faster the pressure is rising at that time, i.e. dP/dt has reached a higher level, and it will take longer from it is electrically activated until it generates force exceeding the higher dP/dt . Hence, the duration from electrical activation to onset shortening is prolonged in late activated regions compared to early activated regions. However, the plots in Fig. 8 also show a fair number of outliers. One possible explanation for these variations is the difficulty in obtaining the targeted placement of the crystals (Fig. 1a). Autopsy after the experiments showed that the crystals had not been implanted at the exact targeted location, especially in the septum. That has likely led to differences in electrical pathways to reach the EMG sensors, which could explain the variations observed in electrical activation delay between animals. Most importantly, it is likely that the crystals were not placed exactly in the imaging plane of a 4-chamber view, and we may therefore not have recorded data from the exact same tissue with the crystals and ultrasound. This is an important source of error and likely to result in some differences in timing of the activation delays. Another possible explanation could be the placement of the ultrasound probe on the heart during imaging. It is possible to alter the regional load and the geometry of the heart if pressure is put on the apex, which would have given us different conditions for the two acquisition methods. For this experiment we attempted to mitigate these effects by using plenty of gel between the probe and the heart. Additionally, the electrical and mechanical activation times were selected manually from the EMG and sonomicrometry traces. The uncertainty of manual selection of

the electrical activation delay between walls was assessed with a standard deviation in Table II. The standard deviation ranged from 0.2 ms to 2.3 ms. Nevertheless, manual selection is a possible cause of error. Automating this selection process could be a subject of future work. For this study it was considered but not prioritized due to the limited amount of data.

The high frame rate ultrasound imaging modality is the cause of some potential sources of error as well. To achieve high frame rate there is a tradeoff between temporal and spatial resolution. Instead of sending a high number of focused beams, which gives a high-quality image, four to six plane waves steered in equidistant directions and parallel receive beamforming were used to create the high frame rate image. In the absence of any compounding [27], the low-resolution image from the plane-wave acquisition will present apparent discontinuities between each acquisition sectors. Those discontinuities are caused by the asymmetric two-way beams of the parallel beamforming approach [28] (Fig. 1a). To avoid errors related to this, we attempted to always keep the cardiac walls within one sector, but image optimization during acquisition was challenging. Another effect of the poor image quality was that it made the LV segmentation in post-processing more demanding. This could potentially have led to inaccurate definition of the endo- and epicardial border. A solution for this could be to acquire high quality B-mode images to use for segmentation.

The algorithm for automatic detection of mechanical activation with CFWI had one important parameter that was manually decided, the CFWI velocity threshold. The effects of changing this parameter was evaluated in Fig. 5. Activation time between walls was plotted against thresholds ranging from 0.05 to 1.05 dB. The plot showed that the activation times remained stable within the used range of 0.25 to 0.6 dB for most cases (5 out of 6). It was also stable below the lower limit of 0.25 dB but became more unstable for values above 0.6 dB. A weakness in the automatic detection algorithm was that for all spatial points where the CFWI velocity reached the threshold within the search area, a mechanical activation was found. This weakness is a possible cause of some of the patchy areas observed in some isochrones and makes the method vulnerable of tracking the wrong point and not the

actual wave front. Developing a more robust algorithm is the subject of future work.

A limitation of TDI is that it does not correct for tethering, and it has been shown that this method is prone to tethering effects of adjacent tissue[29, 30]. The CFWI trace is, as mentioned, similar to the absolute value of the TDI trace. The effects of tethering in this method have not been investigated.

There are several limitations to this study. The reference standard used for comparison for the ultrasound results had a substantially poorer resolution in space. For the crystals, activation was measured only for some locations and segments of the heart, while mechanical activation was estimated for each spatial point of the LV with CFWI. For this study, we acquired only 2D 4-chamber views to estimate the longitudinal motion. However, the longitudinal motion of the heart is typically reduced in the open chest setting. Furthermore, we have attempted to describe a 3D phenomenon with 2D imaging using only 1D motion estimation. This makes our study vulnerable as the mechanical activation wave will propagate in and out of the selected imaging plane. This could possibly explain some discontinuities and noise observed in the isochrones. Furthermore, 1D motion estimation means that we are assuming that the largest motion component is in the axial direction, which may not always hold, especially in the apical regions where the ultrasound beam is not clearly aligned with the cardiac longitudinal direction. In the apical 4-chamber view, such regions include apical and basal regions of the lateral wall. Acquiring more 2D views would mitigate some of the limitations. The best solution would be to image the LV in 3D and derive a 3D map of the mechanical activation, but at this point in time we are not able to achieve a high enough frame rate in 3D with acceptable signal-to-noise ratio to detect this event. CFWI on 3D data, however, has already been shown to work well, and is the subject of ongoing investigation[31]. Further improvement in acquisition and signal processing is needed. Furthermore, studies in human subjects with controlled pacing should be performed to further validate the method before testing feasibility of the method in scenarios where it can truly add value.

V. CONCLUSION

Our study found that mechanical activation measured by CFWI had good agreement with invasive measurements when considering the sequence of the areas being activated. The approximate location of the pacing electrodes could be identified and there were clear differences between the early and the late activated segments of the LV during pacing. The activation delay measurements showed good agreement between methods and an increasing duration from electrical activation to onset shortening for late activated segments compared to early activated segments was found. However, outliers in the dataset were observed. There are several possible explanations for this that need to be investigated further. Nevertheless, this feasibility study shows that this newly developed method has the potential to be a useful, non-invasive tool for the assessment of regional LV mechanical activation mapping.

ACKNOWLEDGMENT

This work was supported by CCI (Center for Cardiological Innovation) supported by the Research Council of Norway.

REFERENCES

- [1] E. Konofagou, W.-N. Lee, J. Luo, J. Provost, and J. Vappou, "Physiologic cardiovascular strain and intrinsic wave imaging," *Annual Review of Biomedical Engineering*, vol. 13, pp. 477-505, 2011.
- [2] A. P. Voorhees and H. C. Han, "Biomechanics of cardiac function," *Comprehensive Physiology*, vol. 5, no. 4, pp. 1623-1644, 2011.
- [3] J. Provost *et al.*, "Electromechanical wave imaging for arrhythmias," *Physics in Medicine & Biology*, vol. 56, no. 22, p. L1, 2011.
- [4] D. A. Auger *et al.*, "Imaging left-ventricular mechanical activation in heart failure patients using cine DENSE MRI: Validation and implications for cardiac resynchronization therapy," *Journal of Magnetic Resonance Imaging*, vol. 46, no. 3, pp. 887-896, 2017.
- [5] K. Russell *et al.*, "Evaluation of left ventricular dyssynchrony by onset of active myocardial force generation: a novel method that differentiates between electrical and mechanical etiologies," *Circulation: Cardiovascular Imaging*, vol. 3, no. 4, p. 405, 2010.
- [6] A. Costet *et al.*, "Non-invasive characterization of focal arrhythmia with electromechanical wave imaging in vivo," *Ultrasound in medicine & biology*, vol. 44, no. 11, pp. 2241-2249, 2018.
- [7] L. Melki *et al.*, "Localization of Accessory Pathways in Pediatric Patients With Wolff-Parkinson-White Syndrome Using 3D-Rendered Electromechanical Wave Imaging," *JACC: Clinical Electrophysiology*, 2019.
- [8] J. Provost, A. Gambhir, J. Vest, H. Garan, and E. E. Konofagou, "A clinical feasibility study of atrial and ventricular electromechanical wave imaging," *Heart Rhythm*, vol. 10, no. 6, pp. 856-862, 2013.
- [9] Y. Wang *et al.*, "Noninvasive electroanatomic mapping of human ventricular arrhythmias with electrocardiographic imaging," *Science translational medicine*, vol. 3, no. 98, pp. 98ra84-98ra84, 2011.
- [10] C. Ramanathan, R. N. Ghanem, P. Jia, K. Ryu, and Y. Rudy, "Noninvasive electrocardiographic imaging for cardiac electrophysiology and arrhythmia," *Nature medicine*, vol. 10, no. 4, p. 422, 2004.
- [11] B. T. Wyman, W. C. Hunter, F. W. Prinzen, and E. R. McVeigh, "Mapping propagation of mechanical activation in the paced heart with MRI tagging," *American Journal of Physiology-Heart and Circulatory Physiology*, vol. 276, no. 3, pp. H881-H891, 1999.
- [12] A. Costet *et al.*, "Electromechanical wave imaging of biologically and electrically paced canine hearts in vivo," *Ultrasound in medicine & biology*, vol. 40, no. 1, pp. 177-187, 2014.
- [13] M. Tanter and M. Fink, "Ultrafast imaging in biomedical ultrasound," *IEEE transactions on ultrasonics, ferroelectrics, and frequency control*, vol. 61, no. 1, pp. 102-119, 2014.
- [14] B. Brekke *et al.*, "Ultra-high frame rate tissue Doppler imaging," *Ultrasound in medicine & biology*, vol. 40, no. 1, pp. 222-231, 2014.
- [15] J. Grondin *et al.*, "Validation of electromechanical wave imaging in a canine model during pacing and sinus rhythm," *Heart rhythm*, vol. 13, no. 11, pp. 2221-2227, 2016.
- [16] J. Provost, W.-N. Lee, K. Fujikura, and E. E. Konofagou, "Electromechanical wave imaging of normal and ischemic hearts in vivo," *IEEE transactions on medical imaging*, vol. 29, no. 3, pp. 625-635, 2010.
- [17] L. C. N. Lervik *et al.*, "Myocardial Strain Rate by Anatomic Doppler Spectrum: First Clinical Experience Using Retrospective Spectral Tissue Doppler from Ultra-High Frame Rate Imaging," *Ultrasound in medicine & biology*, vol. 43, no. 9, pp. 1919-1929, 2017.
- [18] C. Kasai, K. Namekawa, A. Koyano, and R. Omoto, "Real-time two-dimensional blood flow imaging using an autocorrelation technique," *IEEE Transactions on sonics and ultrasonics*, vol. 32, no. 3, pp. 458-464, 1985.

- [19] F. Viola and W. F. Walker, "A comparison of the performance of time-delay estimators in medical ultrasound," *IEEE transactions on ultrasonics, ferroelectrics, and frequency control*, vol. 50, no. 4, pp. 392-401, 2003.
- [20] S. Salles, H. Torp, S. A. Aase, and T. G. Bjåstad, "Clutter filter wave imaging: A new way to visualize and detect mechanical waves propagation," in *Ultrasonics Symposium (IUS), 2017 IEEE International*, 2017, pp. 1-4: IEEE.
- [21] E. E. Konofagou and J. Provost, "Electromechanical wave imaging for noninvasive mapping of the 3D electrical activation sequence in canines and humans in vivo," *Journal of biomechanics*, vol. 45, no. 5, pp. 856-864, 2012.
- [22] B. A. Coppola, J. W. Covell, A. D. McCulloch, and J. H. Omens, "Asynchrony of ventricular activation affects magnitude and timing of fiber stretch in late-activated regions of the canine heart," *American Journal of Physiology-Heart and Circulatory Physiology*, vol. 293, no. 1, pp. H754-H761, 2007.
- [23] E. W. Remme *et al.*, "Mechanisms of preejection and postejection velocity spikes in left ventricular myocardium: interaction between wall deformation and valve events," *Circulation*, vol. 118, no. 4, pp. 373-380, 2008.
- [24] K. Russell *et al.*, "Mechanism of prolonged electromechanical delay in late activated myocardium during left bundle branch block," *American Journal of Physiology-Heart and Circulatory Physiology*, vol. 301, no. 6, pp. H2334-H2343, 2011.
- [25] J. Provost, W.-N. Lee, K. Fujikura, and E. E. Konofagou, "Imaging the electromechanical activity of the heart in vivo," *Proceedings of the National Academy of Sciences*, vol. 108, no. 21, pp. 8565-8570, 2011.
- [26] D. Durrer, R. T. Dam, G. Freud, M. Janse, F. Meijler, and R. Arzbaecher, "Total excitation of the isolated human heart," *Circulation*, vol. 41, pp. 899-912, 1970.
- [27] G. Montaldo, M. Tanter, J. Bercoff, N. Benech, and M. Fink, "Coherent plane-wave compounding for very high frame rate ultrasonography and transient elastography," *IEEE transactions on ultrasonics, ferroelectrics, and frequency control*, vol. 56, no. 3, pp. 489-506, 2009.
- [28] T. Hergum, T. Bjastad, K. Kristoffersen, and H. Torp, "Parallel beamforming using synthetic transmit beams," *IEEE transactions on ultrasonics, ferroelectrics, and frequency control*, vol. 54, no. 2, pp. 271-280, 2007.
- [29] T. Edvardsen, H. Skulstad, S. Aakhus, S. Urheim, and H. Ihlen, "Regional myocardial systolic function during acute myocardial ischemia assessed by strain Doppler echocardiography," *Journal of the American College of Cardiology*, vol. 37, no. 3, pp. 726-730, 2001.
- [30] T. Edvardsen, B. L. Gerber, J. Garot, D. A. Bluemke, J. A. Lima, and O. A. Smiseth, "Quantitative assessment of intrinsic regional myocardial deformation by Doppler strain rate echocardiography in humans: validation against three-dimensional tagged magnetic resonance imaging," *Circulation*, vol. 106, no. 1, pp. 50-56, 2002.
- [31] S. Salles, A. Rodriguez-Molares, T. Bjastad, S. A. Aase, and H. Torp, "3D myocardial mechanical wave measurements using high frame rate ultrasound imaging and Clutter filter wave imaging: Towards a 3D myocardial elasticity mapping," in *Ultrasonics Symposium (IUS), 2017 IEEE International*, 2017, pp. 1-1: IEEE.